Chemotherapy-Induced Collagen IV Drives Cancer Cell Motility through Activation of Src and Focal Adhesion Kinase

Jackson P. Fatherree[1], Justinne R. Guarin[1], Rachel A. McGinn[1], Stephen P. Naber[2], and Madeleine J. Oudin[1]

ABSTRACT

Triple-negative breast cancer (TNBC) is the most aggressive and deadly subtype of breast cancer, accounting for 30,000 cases annually in the United States. While there are several clinical trials ongoing to identify new agents to treat TNBC, the majority of patients with TNBC are treated with anthracycline- or taxane-based chemotherapies in the neoadjuvant setting, followed by surgical resection and adjuvant chemotherapy. While many patients respond well to this approach, as many as 25% will suffer local or metastatic recurrence within 5 years. Understanding the mechanisms that drive recurrence after chemotherapy treatment is critical to improving survival for patients with TNBC. It is well established that the extracellular matrix (ECM), which provides structure and support to tissues, is a major driver of tumor growth, local invasion, and dissemination of cancer cells to distant metastatic sites. In the present study, we show that decellularized ECM (dECM) obtained from chemotherapy-treated mice increases motility of treatment-naïve breast cancer cells compared with vehicle-treated dECM. Tandem-mass–tag proteomics revealed that anthracycline- and taxane-based chemotherapies induce drug-specific changes in tumor ECM composition. The basement membrane protein collagen IV was significantly upregulated in the ECM of chemotherapy-treated mice and patients treated with neoadjuvant chemotherapy. Collagen IV drove invasion via activation of Src and focal adhesion kinase signaling downstream of integrin α1 and α2, and inhibition of collagen IV–driven signaling decreased motility in chemotherapy-treated dECM. These studies provide a novel mechanism by which chemotherapy may induce metastasis via its effects on ECM composition.

Significance: Cytotoxic chemotherapy induces significant changes in the composition of tumor ECM, inducing a more invasive and aggressive phenotype in residual tumor cells following chemotherapy.

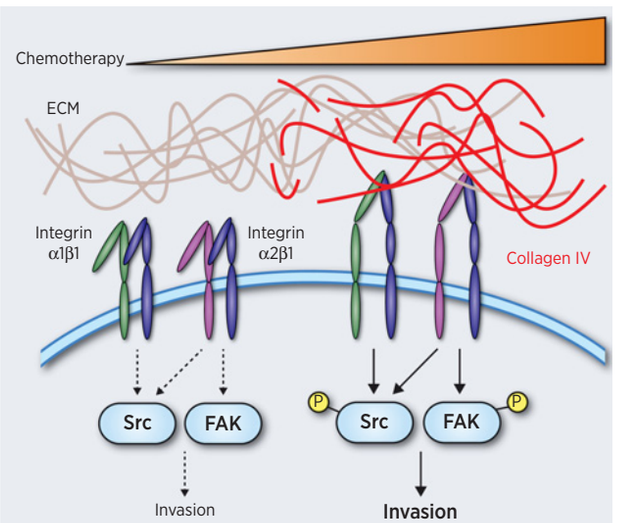

Chemotherapy changes the composition of the extracellular matrix of TNBC, leading to increased abundance of collagen IV and cell invasion via Src/FAK activation downstream of integrin α1/2.

Introduction

Triple-negative breast cancer (TNBC) accounts for approximately 15% to 20% of all breast cancers and is associated with high rates of metastasis and poor overall survival (1). This disease is more prevalent than other subtypes in African-American and premenopausal women, and represents a significant public health concern (1). While other breast cancer subtypes respond well to therapies targeting estrogen receptor (ER), progesterone receptor (PR), or the receptor tyrosine kinase HER2, TNBC remains extremely difficult to treat due to the lack of targetable driver mutations (2). There are several clinical trials ongoing to identify new agents to treat TNBC. The PD-L1 inhibitor atezolizumab was recently approved for TNBC in combination with paclitaxel, but less than 40% of patients with TNBC express PD-L1 and are eligible for this therapy (3). As such, the current standard of care in TNBC is surgical resection followed by cytotoxic chemotherapy, with an increasing number of patients receiving neoadjuvant chemotherapy (NAC) prior to surgery (4). NAC in TNBC consists of a combination of anthracyclines, alkylators, and taxanes; the most common regimen consists of four cycles of concurrent doxorubicin (Adriamycin) and cyclophosphamide, followed by four cycles of paclitaxel (Taxol), hereafter referred to as AC-T (5). While NAC increases the likelihood of pathologic complete response in patients with TNBC, clinical trials have shown that NAC does not improve overall or disease-free survival (6). These clinical observations imply that in a subset of

[1]Department of Biomedical Engineering, Tufts School of Engineering, Tufts University, Medford, Massachusetts. [2]Department of Pathology and Laboratory Medicine, Tufts Medical Center, Boston, Massachusetts.

Note: Supplementary data for this article are available at Cancer Research Online (http://cancerres.aacrjournals.org/).

Corresponding Author: Madeleine J. Oudin, Science & Engineering Complex, 200 College Avenue, Medford, MA 02155. Phone: 617-627-2580; E-mail: madeleine.oudin@tufts.edu

Cancer Res 2022;82:2031–44

doi: 10.1158/0008-5472.CAN-21-1823

patients, effects on tumor cell proliferation and growth do not correlate with suppression of local invasion, which eventually leads to distant metastases.

There is a growing body of evidence indicating that cytotoxic chemotherapy may induce tumor intrinsic and extrinsic changes that promote cancer cell survival and dissemination (7), a phenomenon termed "chemotherapy-induced metastasis". Gene expression analysis of patients with breast cancer following NAC reveals an enrichment for highly invasive, stem-like gene signatures in a subset of postchemotherapy tumors (8). TNBC tumors with low proliferation gene expression signatures and high cell migration gene expression signatures were significantly less likely to achieve pathologic complete response to NAC (9). Within the tumor microenvironment (TME), it is well established that paclitaxel induces tumor angiogenesis by recruiting endothelial progenitor cells (10, 11). In addition, paclitaxel-induced inflammation promotes the recruitment and outgrowth of myeloid progenitor cells, which further support tumor angiogenesis (12). Paclitaxel treatment also stimulates production of epithelial-derived chemoattractants, including colony stimulating factor 1 and IL34, leading to increased recruitment and infiltration of tumor-associated macrophages (13). Doxorubicin can promote chemotherapy-induced metastasis by inducing vascular leakage, leading to recruitment of myeloid-derived cells to the primary tumor (14). Finally, both paclitaxel and doxorubicin have been shown to promote myofibroblastic activation of fibroblasts in the TME (15). Importantly, many of the stromal cell types implicated in TME-mediated chemotherapy-induced metastasis also dynamically degrade, remodel, and secrete extracellular matrix (ECM). Given the role of the ECM in driving local invasion and metastasis (16), further investigation into the role of tumor ECM in chemotherapy-induced metastasis is warranted.

The ECM, which provides biochemical and biophysical signals to all solid tissues, is a major driver of tumorigenesis and metastasis in breast cancer (17). ECM organization and composition is commonly dysregulated in solid tumors (18). In breast cancer, increased collagen I deposition and fiber alignment is associated with increased invasiveness and high-grade tumors (19, 20). Recent advances in the field of ECM proteomics have revealed exceptional heterogeneity in the tumor matrisome (21) and described significant differences in the contributions of cancer cells and stromal cells to ECM deposition (22). It is now understood that the structure and composition of the tumor ECM is the result of dynamic interplay between fibroblasts, macrophages, endothelial cells, and cancer cells (23–26). As each of these cell types is directly or indirectly affected by cytotoxic chemotherapy, we hypothesized that chemotherapy would induce substantial changes in the composition of tumor ECM.

Unbiased investigation of the role of ECM in driving cancer cell phenotypes has been an ongoing challenge. *In vitro* investigation of cell–ECM interactions typically involves exposing cells to a single ECM substrate and assaying adhesion, proliferation or invasion. While these tools are useful for dissecting the signals underlying ECM-driven phenotypes, they fail to capture the complexity of native ECM in terms of both composition and three-dimensional (3D) structure. More complex tools have been developed to recapitulate native ECM, including the use of Matrigel (27), cell-derived matrices (28), and synthetic ECM scaffolds (29). However, these tools fail to replicate the complexity and heterogeneity of the *in vivo* ECM, leading some researchers to incorporate *ex vivo* decellularized tissue as a model for native ECM (30). Leveraging these techniques, we recently published an experimental pipeline for interrogating the effect of native whole-tissue ECM from different disease states on cancer cells (31). By isolating native intact decellularized ECM (dECM) directly from primary tissues and employing them as scaffolds for *ex vivo* studies, we are able to observe whole-tissue ECM-driven cellular phenotypes, irrespective of the source of ECM in the TME.

In this study, we use this approach to demonstrate increased cancer cell motility driven by chemotherapy-treated tumor ECM, which is associated with significant alterations in ECM composition. We identify collagen IV as a major driver of TNBC cell invasion that is induced by chemotherapy in both mice and humans. We further show that collagen IV–driven Src and focal adhesion kinase (FAK) signaling can be targeted to suppress chemotherapy-associated ECM-driven invasion in TNBC. These findings represent the first ECM-based mechanism of chemotherapy-induced metastasis and provide a rationale for targeting Src and FAK signaling in combination with neoadjuvant chemotherapy.

Materials and Methods

Mice

All animal studies were reviewed and approved by the Tufts University (Boston, MA) Institutional Animal Care and Use Committee. Female transgenic mice bearing the polyomavirus middle T antigen under control of the mouse mammary tumor virus promoter (MMTV-PyMT) were obtained from The Jackson Laboratory. MMTV-PyMT mice were grown until overall tumor burden reached 500 mm^3 at about 10 to 12 weeks of age before being randomized into chemotherapy treatment groups. Paclitaxel (Taxol) was resuspended in 5% dimethyl sulfoxide, 40% polyethylene glycol 3000, and 5% Tween 80 in dH_2O and administered intraperitoneally at 10 mg/kg. Doxorubicin (Adriamycin) was dissolved in PBS and administered intravenously at 5 mg/kg. Appropriate vehicle controls for each drug were included in the control group. All drugs were administered for four cycles given every 5 days. Tumor burden was monitored using digital calipers at each treatment. Three days after the final treatment, mice were euthanized, and tumors and lungs were excised for further study.

Antibodies and inhibitors

Primary antibodies used in this study include: α-fibronectin (ab2413; Abcam), α-tubulin (DM1A; Sigma-Aldrich), α-GAPDH (1:2500, 14C10; Cell Signaling Technology), α-collagen IV (1:100, ab6586; Abcam), α-phospho-Src (2101; Cell Signaling Technology), α-Src (36D10; Cell Signaling Technology), α-phospho-FAK (3283; Cell Signaling Technology), α-FAK (D5O7U; Cell Signaling Technology), α-phospho-Erk1/2 (4370; Cell Signaling Technology), α-Erk1/2 (4695; Cell Signaling Technology), α-phospho-Akt (9271; Cell Signaling Technology), α-Akt (4691; Cell Signaling Technology), α-integrin α1 (ITGA1; ab181434; Abcam), and α-integrin α2 (ITGA2; ab181548; Abcam) All antibodies were used at a concentration of 1:1000 unless indicated otherwise. Pharmacologic inhibitors include: dasatinib (S1021; Selleck Chemicals) and defactinib (S7654; Selleck Chemicals).

Cell culture

MDA-MB-231 cells were obtained from ATCC and cultured in DMEM with 10% FBS and 1% penicillin–streptomycin–glutamine. We generated fluorescently labeled versions of the MDA-MB-231 cells by transduction of TurboGFP-containing lentiviral particles (SHC003V; Sigma-Aldrich), these cells are labeled 231-GFP. GFP-labeled PyMT tumor-derived (PyMT-GFP) cells were a gift from Prof. Richard Hynes' lab at Massachusetts Institute of Technology

(MIT; Cambridge, MA) and were cultured in a 1:1 mix of DMEM and Ham's F-12 Nutrient Mixture containing 2% FBS, 1% BSA (A2153–50G; Sigma-Aldrich), EGF (10 ng/mL, PHG0313; Thermo Fisher Scientific), insulin (10 μg/mL, 12585014; Thermo Fisher Scientific), and 1% penicillin–streptomycin–glutamine. Cells were monitored for *Mycoplasma* contamination by PCR using the Universal *Mycoplasma* Detection Kit (30-1012 K; ATCC). Only *Mycoplasma*-negative cells were used in this study and all experiments were conducted within 15 passages of thawing.

Isolation of dECM scaffolds

Tumor-derived dECM scaffolds were produced as described previously (31). Briefly, tumors dissected from MMTV-PyMT mice were submerged in 0.1% SDS in PBS (w/v) solution with agitation for 3 to 5 days, replacing the solution twice daily. Once the tissue had turned completely white, tissues were moved to 0.05% Triton X-100 in PBS solution for 3 hours, followed by washing in dH_2O for 48 hours to remove residual detergents. To assess decellularization, dECM scaffolds were paraffin embedded, sectioned, and hematoxylin and eosin (H&E) stained.

Protein isolation

dECM, intact tumors, or cell pellets were lysed in 25 mmol/L tris, 150 mmol/L NaCl, 10% glycerol, 1% NP-40, and 0.5 mol/L EDTA with 1× protease Mini-complete protease inhibitor (04693124001; Roche) and 1× phosphatase inhibitor cocktail (4906845001; Roche) at 4°C. In the case of dECM and intact tumors, mechanical homogenization was achieved using the Bead-Bug 3 Place Microtube Homogenizer (D1030; Benchmark Scientific). The resulting homogenate was then centrifuged at 21,000 g for 10 minutes at 4°C and the supernatant was stored at −20°C for subsequent analysis.

dECM reseeding experiments

Reseeding experiments were performed as described previously (31). Five-millimeter pieces of dECM scaffold were cut and conditioned in complete cell culture media for 48 hours. On the morning of the experiment, tissues were reseeded with 250,000 231-GFP or PyMT-GFP cells and incubated at 37°C for 6 hours. Reseeded tissue was then moved to fresh media, stabilized, and imaged for 16 hours, capturing images every 20 minutes. For inhibitor experiments, vehicle controls or small-molecule inhibitors were added to the media just before imaging began. Cells were then tracked using VW-9000 Video Editing/Analysis Software (Keyence) based on movement of the main cell body, and speed was calculated using a custom MATLAB script vR2018a (MathWorks). Data presented are the result of at least three independent experiments with five fields of view imaged per experiment and 4 to 8 cells tracked per field of view.

LC/MS-MS analysis

Samples were prepared as described previously (31). Briefly, dECM homogenate was denatured in 8 mol/L urea and 10 mmol/L dithiothreitol, alkylated with 25 mmol/L iodoacetamide, and deglycosylated with peptide *N*-glycosidase F (P0704S; New England Biolabs). Samples were then digested sequentially, first with endoproteinase LysC (125-05061; Wako Chemicals USA), then trypsin (PR- V5113; Promega). Samples were acidified with 50% trifluoroacetic acid and labeled with TMT10plex (90110; Thermo Fisher Scientific) according to the manufacturer's instructions. Labeled peptides were fractionated via high-pH reverse-phase high-performance liquid chromatography (Thermo Easy nLC1000; Thermo Fisher Scientific) using a precolumn (made in house, 6 cm of 10-μmol/L C18) and a self-pack 5-μmol/L tip analytical column (12 cm of 5-μmol/L C18; New Objective) over a 140-minute gradient before nanoelectrospray using a Q Exactive HF-X mass spectrometer (Thermo Fisher Scientific). Solvent A was 0.1% formic acid, and solvent B was 80% ACN/0.1% formic acid. The gradient conditions were 2% to 10% B (0 to 3 minutes), 10% to 30% B (3 to 107 minutes), 30% to 40% B (107 to 121 minutes), 40% to 60% B (121 to 126 minutes), 60% to 100% B (126 to 127 minutes), 100% B (127 to 137 minutes), 100% to 0% B (137 to 138 minutes), and 0% B (138 to 140 minutes), and the mass spectrometer was operated in a data-dependent mode. The parameters for the full-scan MS were resolution of 60,000 across 350 to 2,000 mass/charge ratio (m/z), automatic gain control 3 × 106, and maximum ion injection time of 50 milliseconds. The full-scan MS was followed by tandem mass spectrometry (MS/MS) for the top 15 precursor ions in each cycle with a normalized collision energy of 34 and dynamic exclusion of 30 seconds.

Breast cancer patient mRNA analysis

For analysis of collagen IV gene expression, mRNA data was downloaded from the Molecular Taxonomy of Breast Cancer International Consortium (METABRIC) database (cBioportal.org). From these data, we selected patients with TNBC based on ER, PR, and HER2 positivity. Patients were stratified based on whether they had received chemotherapy or not, and expression of all six collagen IV genes was compared between these two groups. To determine how age influences collagen IV in TNBC, the average expression of all six collagen IV genes was quantified and compared with the patients' age at diagnosis.

For analysis of patient survival, we used kmplot.com, a meta-analysis tool that allows querying a large collection of breast cancer patient RNA microarray datasets. Either patients with TNBC or all patients with breast cancer were used for analysis and stratified based on high (above median) or low (below median) expression of *COL4A1-5*, with data were reported as probability of recurrence. Patients were further selected for therapy status to determine associations between chemotherapy, collagen IV, and patient outcomes.

Western blotting

Protein lysates were separated using SDS-PAGE on a 12% polyacrylamide gel. Proteins were transferred to a nitrocellulose membrane using a TransBlot Turbo Transfer system (Bio-Rad). Membranes were blocked in 5% nonfat dry milk in TBS with 0.05% tween 20 and incubated in primary antibody overnight at 4°C with rocking. Antibody binding was visualized using horseradish peroxidase–conjugated secondary antibodies (Jackson ImmunoResearch). Imaging was performed using a ChemiDoc MP imaging system (12003154; Bio-Rad).

IHC

Tissue fixation, processing, and sectioning was performed as previously described (31). MMTV-PyMT tumors were fixed in 4% paraformaldehyde in PBS, embedded in paraffin, and sectioned into 10-μm sections. Human TNBC samples were obtained from the Tufts Medical Center (Boston, MA) Biorepository as deidentified formalin-fixed, paraffin-embedded 5-μm sections. For H&E staining, sections were deparaffinized, hydrated, stained with hematoxylin (GHS280; Sigma-Aldrich), and counterstained with eosin (HT110180; Sigma-Aldrich). Stained sections were mounted in toluene (SP15–500, Thermo Fisher Scientific). For immunofluorescence, tissue sections were deparaffinized and antigen retrieval was performed in Citra Plus solution (HK057; Biogenex). Sections were then blocked in PBS with 0.5% tween 20 and 10% donkey serum and incubated with primary antibodies overnight at 4°C. The next day, sections were incubated

with fluorophore-conjugated secondary antibodies and 4′,6-Diamidino-2-phenylindole (DAPI; D1306; Thermo Fisher Scientific) to stain cell nuclei. Sections were mounted in Fluoromount mounting medium (00-4958-02; Thermo Fisher Scientific) and imaged using a Keyence BZ-X710 microscope (Keyence) capturing five fields of view per section. Quantification of ECM signal was performed by measuring mean fluorescent intensity and quantification of DAPI positivity was performed by measuring $DAPI^{+}$ maxima using ImageJ (NIH, Bethesda, MD).

3D invasion assays

Spheroid invasion assays were performed as described previously (32). 1,000 231-GFP or 2,000 PyMT-GFP cells were seeded in round-bottom, low-attachment 96-well plates and centrifuged at 3,000 g for 3 minutes to promote spheroid formation. Spheroids were allowed to grow for three days before addition of an ECM mixture of 1 mg/mL collagen I (354236; Corning), 10 mmol/L NaOH, 7.5% 10X DMEM, and 50% DMEM with or without 20 μg/mL native human collagen IV (ab7536; Abcam). Once ECM had solidified, 50 μL of culture media was added to maintain moisture and humidity in the well. In inhibitor studies, this media included DMSO as a vehicle control or small molecule inhibitors. Spheroids were imaged in 3D on the day of ECM addition and after 4 days of growth using a Keyence BZ-X710 microscope (Keyence).

For 3D single-cell invasion assays, 20,000 231-GFP or PyMT-GFP cells were suspended in ECM mixture described above with or without 20 μg/mL collagen IV and seeded into 48-well tissue culture plates. Once ECM had solidified, 50 μL of culture media to maintain moisture and humidity in the well. In inhibitor studies, cells were treated with DMSO as a vehicle control or small molecule inhibitors 1 hour before imaging. Cells with imaged live in 3D over 16 hours using a Keyence BZ-X710 microscope and invasive speed was quantified as in reseeding experiments.

RNA isolation and qPCR

RNA was isolated using a Quick-RNA MiniPrep Plus Kit (Zymo Research) according to the manufacturer's instructions. cDNA was synthesized from 500 ng total RNA using SuperScript IV reverse transcriptase (Invitrogen). PCR was conducted using 0.3 μmol/L gene-specific primers and Power UP SYBR Green PCR master mix (Applied Biosystems). Primers used include *ITGA1*-forward (5′-AGAATGCAGCACTCAACTGG-3′), *ITGA1*-reverse (5′-TGCAACAAGTACCTCTTCGG), *ITGA2*-forward (5′-ATCATTCTCCCTGCCGGTTG-3′), *ITGA2*-reverse (5′-TTGGAAACTGAGAGACGCCTG-3′), *SDHA*-forward (5′-TG-GGAACAAGAGGGCATCTG-3′), *SDHA*-reverse (5′-CCACCACT-GCATCAAATTCATG-3′), *HPRT*-forward (5′-TCAGGCAGTATAATCCAAAGATGGT-3′), *HPRT*-reverse (5′-AGTCTGGCTTATATCCAACACTTCG-3′). *SDHA* and *HPRT* were used as internal controls. Integrin gene expression was quantified using $\Delta\Delta C_t$ method normalizing to the appropriate control.

siRNA transfection

ON-TARGETplus SMARTpool siRNA targeting *ITGA1* and *ITGA2* were obtained from Horizon Discovery Inc. with the following sequences: *ITGA1–1* (5′-AGACAAAUAUCACGAAGUU-3′), *ITGA1–2* (5′-GGAUUUAAAUGGUGACGGU-3′), *ITGA1–3* (5′-CAGCUAUAACCGAGGAAAU-3′), *ITGA1–4* (5′-CCUUCUACAUGUUGGACAA-3′), *ITGA2–1* (5′-GAACGGGACUUUCGCAUCA-3′), *ITGA2–2* (5′-GAAACGCCCUUGAUACUAA-3′), *ITGA-3* (5′-GUUCAGACCUACUAAGCAA-3′), *ITGA2–4* (5′-AAACAAGGCUGAUAAUUUG-3′). Hundred thousand TNBC cells were seeded into six-well tissue culture plates. Cells were transfected with 30 nmol/L of a nontargeting control siRNA or siRNA targeted to relevant integrin mRNA transcripts. Transfections were performed with Lipofectamine RNAiMAX transfection reagent (Invitrogen) and cells were used for downstream analysis 48 hours posttransfection.

Statistical analysis

Statistical analysis and visualization were performed using GraphPad Prism v8.4.3 unless indicated otherwise. To compare two groups, an unpaired Student t test was used where a P value ≤ 0.05 was considered statistically significant. To compare between more than two groups, a one-way ANOVA was performed using a Bonferroni multiple testing correction where a corrected P value ≤ 0.05 was considered statistically significant. For analysis of patient survival, a log-rank test was used where a P value ≤ 0.05 was considered statistically significant.

For proteomics analysis, principal component analysis was performed using MatLab and visualized in GraphPad Prism. Statistical significance of individual proteins was determined with Scaffold 4 (Proteome Software) using a Mann–Whitney test with a Benjamini–Hochberg adjusted α to reflect a FDR of 1%.

Data availability statement

The MS proteomics data have been deposited to the ProteomeXchange Consortium via the PRIDE partner repository with the dataset identifier PXD032002. All other data are available in the main text or the supplemental materials.

Results

Postchemotherapy tumor dECM scaffolds promote TNBC cell motility

To investigate how cytotoxic chemotherapy alters ECM-driven phenotypes in TNBC, we used transgenic MMTV-PyMT mice, an immunocompetent model that faithfully recapitulates the pathology of human TNBC (33). Once overall tumor burden reached 500 mm^3, at about 12 weeks of age, mice were treated every 5 days with four cycles of either paclitaxel (10 mg/kg), delivered intraperitoneally; doxorubicin (5 mg/kg), delivered intravenously; or a vehicle control (Supplementary Fig. S1A). Both treatments significantly slowed tumor growth, but did not induce tumor regression, relative to the vehicle control (Supplementary Fig. S1B). However, neither treatment reduced the number of lung metastases at sacrifice between vehicle- and chemotherapy-treated mice (Supplementary Fig. S1C and S1D).

To study the effect of chemotherapy-treated ECM on cancer cell motility, a necessary feature for local invasion and metastasis, we decellularized PyMT tumors using our recently published method (31) to obtain dECM scaffolds derived from vehicle-, paclitaxel-, or doxorubicin-treated tumors. Decellularization was confirmed by H&E staining, DAPI staining, and Western blot (Supplementary Fig. S2A–S2E). These dECM scaffolds were reseeded with PyMT-GFP cells and imaged live over 16 hours to assay the effect of chemotherapy-treated tumor dECM on cell speed, persistence, and displacement (**Fig. 1A**). Tumor dECM isolated from either paclitaxel- or doxorubicin-treated tumors significantly increased cell speed and net displacement, but not persistence, relative to vehicle-treated tumor dECM (**Fig. 1B–E**). These results suggest that chemotherapy-driven changes in the ECM can drive cancer cell motility, a phenotype that promotes drug resistance, tumor progression, and metastasis.

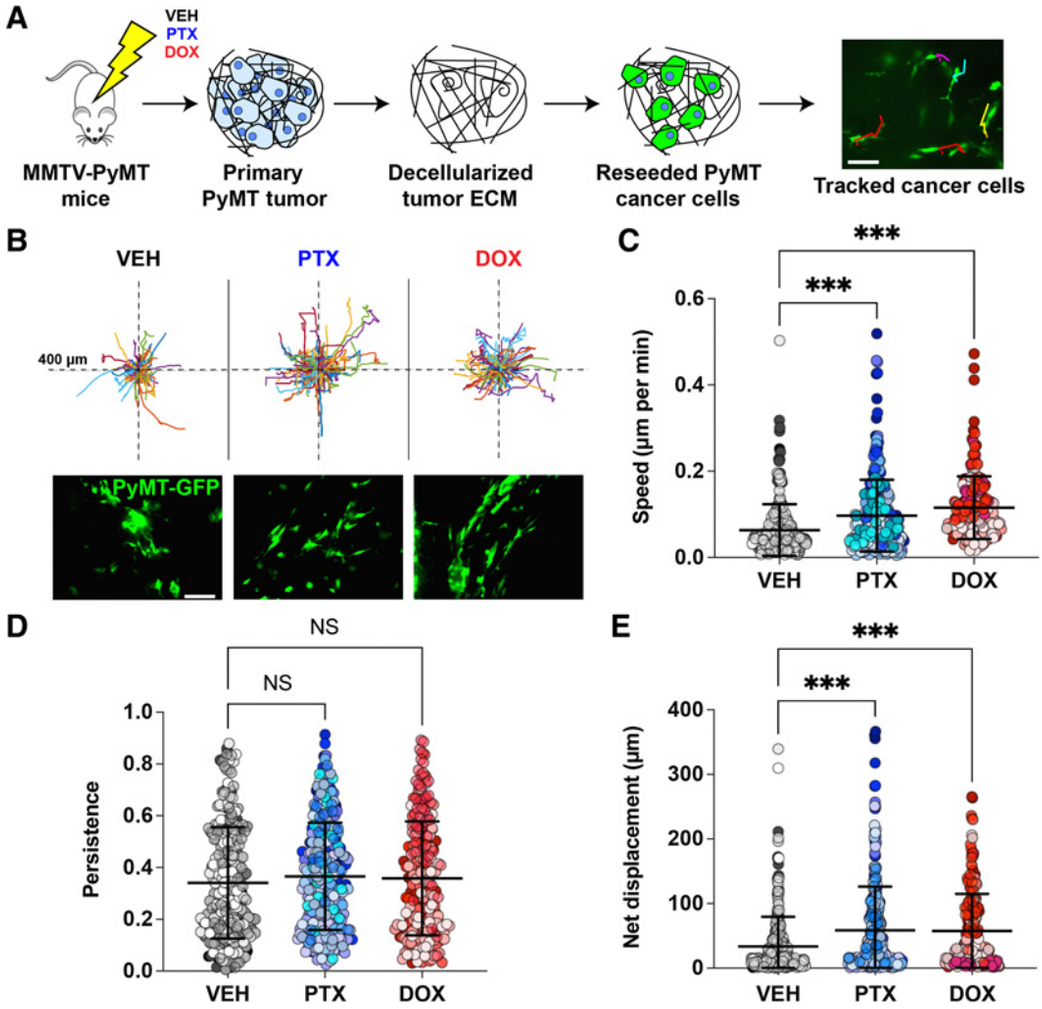

Figure 1.

Chemotherapy-treated dECM promotes motility of PyMT-GFP TNBC cells. **A,** Schematic diagram of experiment. MMTV-PyMT mice were treated with paclitaxel (10 mg/kg), doxorubicin (5 mg/kg), or a vehicle control. Tumors were excised and decellularized to obtain dECM scaffolds. dECM scaffolds were reseeded with PyMT-GFP cells and imaged overnight. Moving cells were tracked to quantify cell speed. Scale bar, 250 μm). **B,** Rose plots visualizing the paths of individual cells on dECM scaffolds (top) and representative frames obtained from reseeding videos of PyMT-GFP cells on dECM from each treatment group (bottom). Scale bar, 250 μm. **C,** Speed of PyMT-GFP cells seeded on dECM from vehicle-, paclitaxel-, and doxorubicin-treated mice. **D,** Persistence of moving cells measured as the ratio between net displacement and total distance traveled. **E,** Net displacement of individual cells over the course of the experiment. Each point represents a single cell over 16 hours. Like-colored points represent cells tracked on the same dECM scaffold. Data show mean ± SD (n = at least 200 cells tracked from at least 5 dECM scaffolds per treatment group). Significance was determined by one-way ANOVA. ***, $P < 0.005$. PTX, paclitaxel; DOX, doxorubicin; VEH, vehicle; min, minute; NS, not significant.

Cytotoxic chemotherapy alters the composition of TNBC tumor ECM

To determine how chemotherapy alters the ECM to promote cancer cell motility, we first set out to understand how chemotherapy alters the amount and organization of tumor ECM. We characterized collagen I and III abundance by picrosirius red staining and collagen I architecture by second-harmonic generation imaging (Supplementary Fig. S2F). Doxorubicin, but not paclitaxel, increased fibrotic area, as stained by collagen I and III, in PyMT tumors (Supplementary Fig. S2G), while neither drug had any effect on collagen I alignment (Supplementary Fig. S2H). These data suggest that changes in ECM structural organization are likely not enough to explain the increased motility observed in both paclitaxel- and doxorubicin-treated dECM scaffolds. We then hypothesized that chemotherapies alter the protein-level composition of tumor matrisome to promote cancer cell motility. To fully characterize the PyMT tumor matrisome, we employed a published proteomics approach (31, 34). Existing dECM scaffolds from vehicle- and chemotherapy-treated tumors were digested to obtain peptides suitable for mass spectrometry analysis. Five vehicle samples were pooled to represent a composite of the PyMT tumor matrisome, and all samples were labeled using unique isobaric tandem-mass tags to enable quantitative comparison of peptide abundance across samples.

We analyzed the resulting dataset by principal component analysis (PCA), which revealed that paclitaxel and doxorubicin induce distinct changes in the composition of tumor ECM (**Fig. 2A**). Proteins

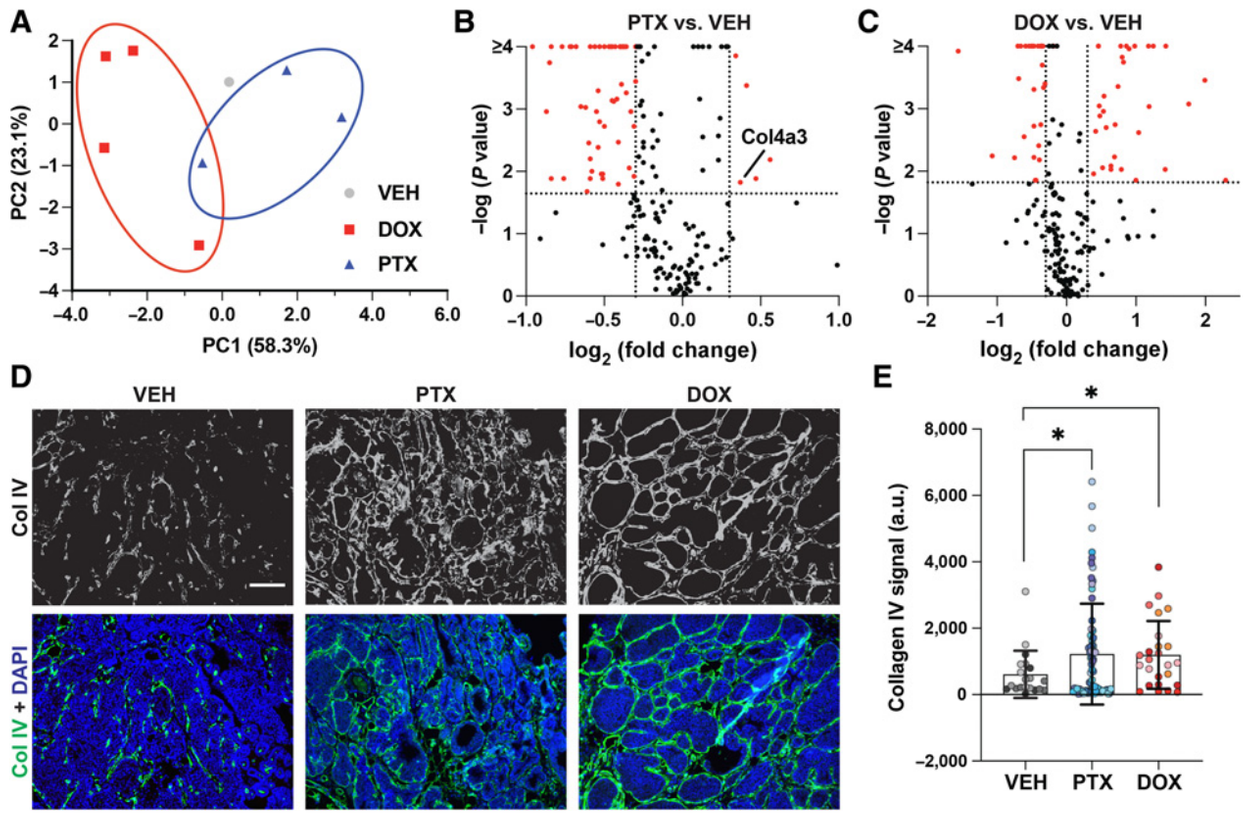

Figure 2.

Collagen IV is upregulated by chemotherapy in MMTV-PyMT tumors. **A,** PCA of proteomics study investigating dECM composition from vehicle-, paclitaxel-, and doxorubicin-treated tumors. **B,** Volcano plot comparing dECM composition of paclitaxel- and vehicle-treated dECM. **C,** Volcano plot comparing dECM composition of doxorubicin- and vehicle-treated dECM. Dotted lines show effect size threshold (vertical) or Benjamini–Hochberg adjusted α (horizontal). **D,** Immunostaining of MMTV-PyMT sections from vehicle-, paclitaxel-, or doxorubicin-treated mice stained for collagen IV and nuclei. Scale bar, 100 μm. **E,** Intensity of collagen IV signal in vehicle-, paclitaxel-, or doxorubicin-treated MMTV-PyMT sections. Like-colored points represent fields of view from the same tissue section and mouse. Data show mean ± SD [n = at least 3 dECM scaffolds (**A–C**) or at least 5 independent mice (**D** and **E**)]. Significance was determined by unpaired t test. *, $P < 0.05$. a.u., arbitrary units; Col IV, collagen IV; DOX, doxorubicin; PTX, paclitaxel; VEH, vehicle.

identified were annotated using publicly available tools to determine changes in matrisome composition. Consistent with previous studies, roughly half of the spectra identified mapped to the known matrisome (Supplementary Fig. S3A; ref. 22). We identified 208 proteins in the PyMT tumor matrisome (Supplementary Fig. S3B), with 59 and 60 differentially regulated proteins in paclitaxel- and doxorubicin-treated dECM, respectively (**Fig. 2B** and **C**; Supplementary Fig. S3C and S3D; Supplementary Data S1). These data constitute the first comprehensive characterization of the chemotherapy-treated TNBC matrisome.

COL4A3, a subunit of collagen IV, was among the top hits in paclitaxel-treated tumor dECM. Collagen IV has been associated with metastatic breast cancer (35), and is known to drive cancer cell invasion (36). Further, cancer-associated fibroblasts produce collagen IV in response to taxane-based chemotherapy *in vitro* (37). Therefore, we chose to investigate if chemotherapy treatment induced an increase in native collagen IV in an independent set of MMTV-PyMT mice. Interestingly, both paclitaxel and doxorubicin treatment significantly increased the abundance of native collagen IV in PyMT tumors (**Fig. 2D** and **E**). Together, these data indicate that cytotoxic chemotherapies cause largely drug-specific alterations in the PyMT tumor matrisome and identify collagen IV as significantly more abundant in chemotherapy-treated mice.

Chemotherapy treatment is associated with increased collagen IV in human TNBC

To determine if collagen IV abundance is also regulated by cytotoxic chemotherapy in human TNBC, we obtained matched diagnostic biopsies and surgical resections from seven patients with TNBC treated at Tufts Medical Center who received AC-T neoadjuvant chemotherapy between diagnosis and surgery. Patient cohort information is available in Supplementary Table S1. After immunostaining sections from diagnostic biopsy (pre–AC-T) and from surgical resections (post–AC-T) to quantify native collagen IV abundance, we found that 4 of 7 patients displayed a large increase in collagen IV abundance, while 3 of 7 patients had slightly reduced collagen IV abundance (**Fig. 3A** and **B**). Collagen IV is encoded by six different genes (*COL4A1* to *A6*), each encoding for a single α chain, which construct 3 heterotrimers (α112, α345, and α556). Importantly, the antibody used in this study is polyclonal and recognizes each of these heterotrimers when in the native conformation. To determine how chemotherapy regulates specific collagen IV α chains, we obtained mRNA expression data of patients with TNBC from the METABRIC (downloaded from cBioportal.org). We found that four out of six collagen IV chains (*COL4A1-4*) were upregulated in chemotherapy-treated patients, while the remaining two chains (*COL4A5/6*) were

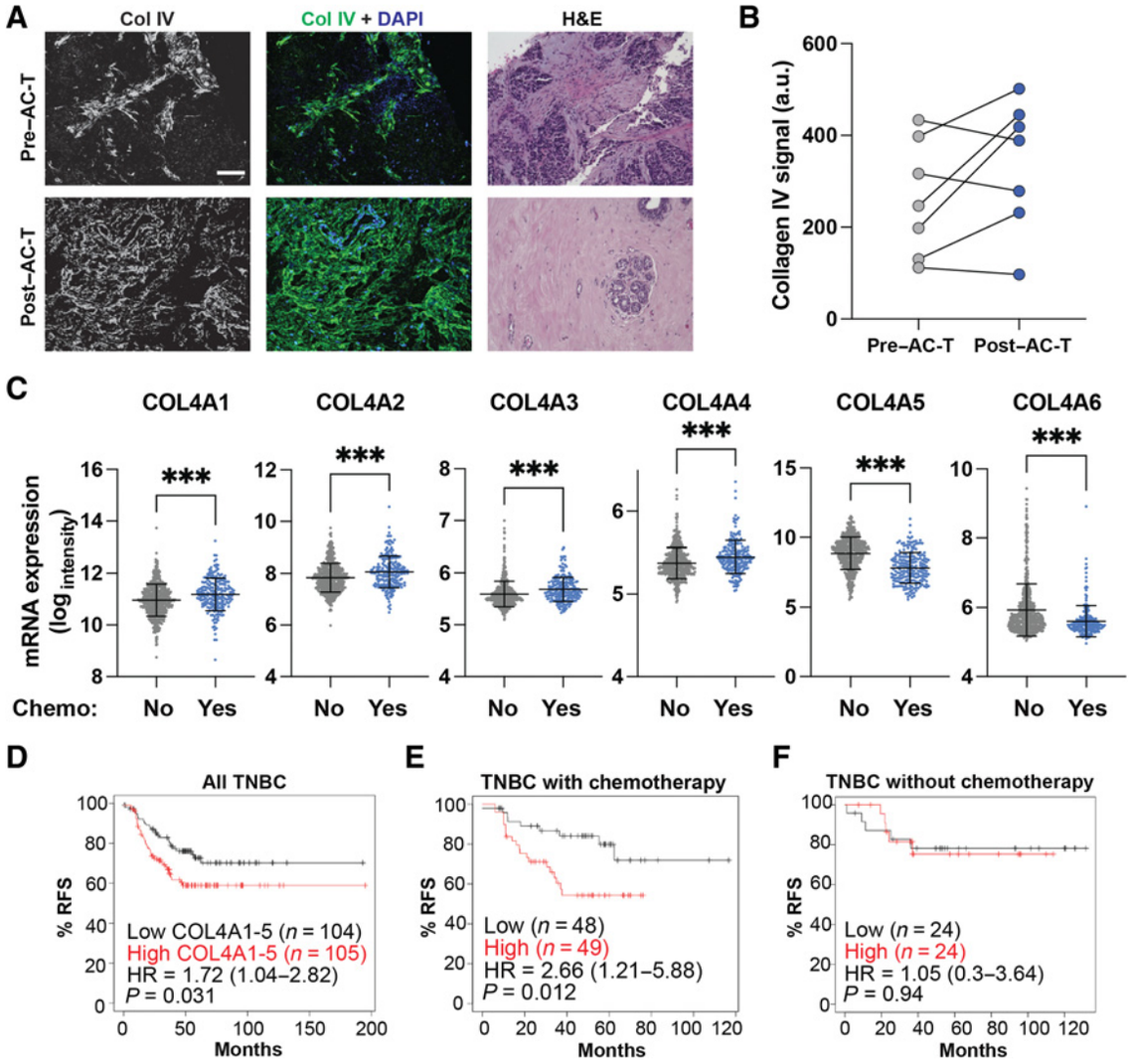

Figure 3.

Collagen IV abundance is increased and associated with poor outcomes in chemotherapy-treated human patients with TNBC. **A,** Immunostaining of human TNBC sections retrieved from diagnostic biopsy (pre–AC-T) and surgical resections (post–AC-T) stained for collagen IV and nuclei. H&E staining for histologic comparison. Scale bar, 100 μm. **B,** Collagen IV signal intensity measured from matched pre– and post–AC-T sections. **C,** mRNA expression data from patients with TNBC with or without chemotherapy (METABRIC) showing expression of collagen IV α chains. **D–F,** Kaplan-Meier curves of all patients with TNBC (**D**), chemotherapy-treated patients with TNBC (**E**), or systemically untreated patients with TNBC (**F**) visualizing patient outcomes based on average expression of five collagen IV α chains (COL4A1-5). Data show mean ± SD [$n = 7$ paired biopsies and surgical resections (**A** and **B**) or 517 untreated vs. 213 chemotherapy-treated patients with TNBC (**C–H**)]. For gene expression, significance was determined by unpaired t test. For survival curves, patients were stratified by median COL4A1-5 expression and significance was determined by log-rank test. ***, $P < 0.005$. a.u., arbitrary units, Col IV, collagen IV; chemo, chemotherapy.

downregulated (**Fig. 3C**). These data serve to validate our hypothesis that chemotherapy can induce an increase in collagen IV in human TNBC, potentially through increases in the α112 and α345 heterotrimers.

Collagen IV expression is associated with poor outcomes among chemotherapy-treated patients with TNBC

To understand the relationship between collagen IV and chemotherapy in a broader clinical context, we interrogated publicly available datasets of TNBC patient outcomes using kmplot.com (38). Patients were stratified based on their average expression of five collagen IV genes (*COL4A1-5*), representing the collagen IV heterotrimers most associated with chemotherapy. Among patients with TNBC, high collagen IV expression was associated with poor recurrence-free survival (RFS; **Fig. 3D**). Interestingly, when we looked deeper into this data, we found that this association was stronger among patients who had received cytotoxic chemotherapy (**Fig. 3E**), while among patients with TNBC who did not receive any systemic chemotherapy, there was no association between collagen IV expression and RFS (**Fig. 3F**), further indicating a link between chemotherapy status, collagen IV, and poor outcomes in TNBC. These trends held true when considering all patients with breast cancer, regardless of hormone receptor status (Supplementary Fig. S4A–S4D). Further analysis of the METABRIC dataset revealed no association between *COL4A1-5*

expression and age, an important covariate of patient survival in TNBC (Supplementary Fig. S4E). Together, these data demonstrate that cytotoxic chemotherapy increases collagen IV abundance in a subset of patients with TNBC, and that this increase may be associated with worse outcomes after chemotherapy treatment.

Collagen IV drives spheroid growth and 3D invasion of TNBC cells

To determine if increased collagen IV abundance explains the increased motility in cells seeded on chemotherapy-treated dECM, we investigated the effect of collagen IV on the growth and invasion of TNBC cells in 3D. We previously described a tunable spheroid model suitable for analyzing the effect of individual ECM proteins on TNBC cell invasion (31, 32), which accurately recapitulates the behavior of tumor cells *in vivo* (39). PyMT-GFP spheroids were grown in collagen I, the most abundant ECM protein in breast tissue, with or without native human collagen IV. PyMT-GFP spheroids grew significantly larger in the presence of collagen IV when compared with the collagen I only control (**Fig. 4A**). We repeated these experiments using GFP-labeled human MDA-MB-231 TNBC cells (231-GFP) and found that collagen IV also increased spheroid growth of these cells (**Fig. 4B**). To confirm that these results are due to increased invasion and not increased proliferation, we used an orthogonal approach where cancer cells were suspended throughout collagen gels with or without collagen IV. These were imaged live over 16 hours to quantify invasion at single-cell resolution in a 3D environment. We found that both PyMT-GFP and 231-GFP cells invade faster in the presence of collagen IV (**Fig. 4C** and **D**). To determine if collagen IV-driven proliferation is a confounding factor, we quantified TNBC cell proliferation in 2D and 3D. By quantifying cell proliferation events from these videos, we found that PyMT-GFP cells proliferated less in collagen IV-containing gels (Supplementary Fig. S5A) compared with the collagen I control. Further, PyMT-GFP cells proliferated at the same rate when seeded on collagen I or collagen IV in 2D (Supplementary Fig. S5B). 231-GFP cells had no proliferative response to collagen IV in 2D or 3D (Supplementary Fig. S5C and S5D). Together, these experiments clearly establish that collagen IV stimulates 3D invasion, but not proliferation, in mouse and human TNBC cells.

Collagen IV induces Src/FAK signaling downstream of α integrins

We next sought to elucidate the molecular pathways underlying collagen IV–driven invasion. Collagen IV has been described to signal through a wide range of pathways depending on the cellular context, including MAPK (40), PI3K (41), Src (42, 43), and FAK (40, 44). To determine which of these signals is mediating collagen IV–driven

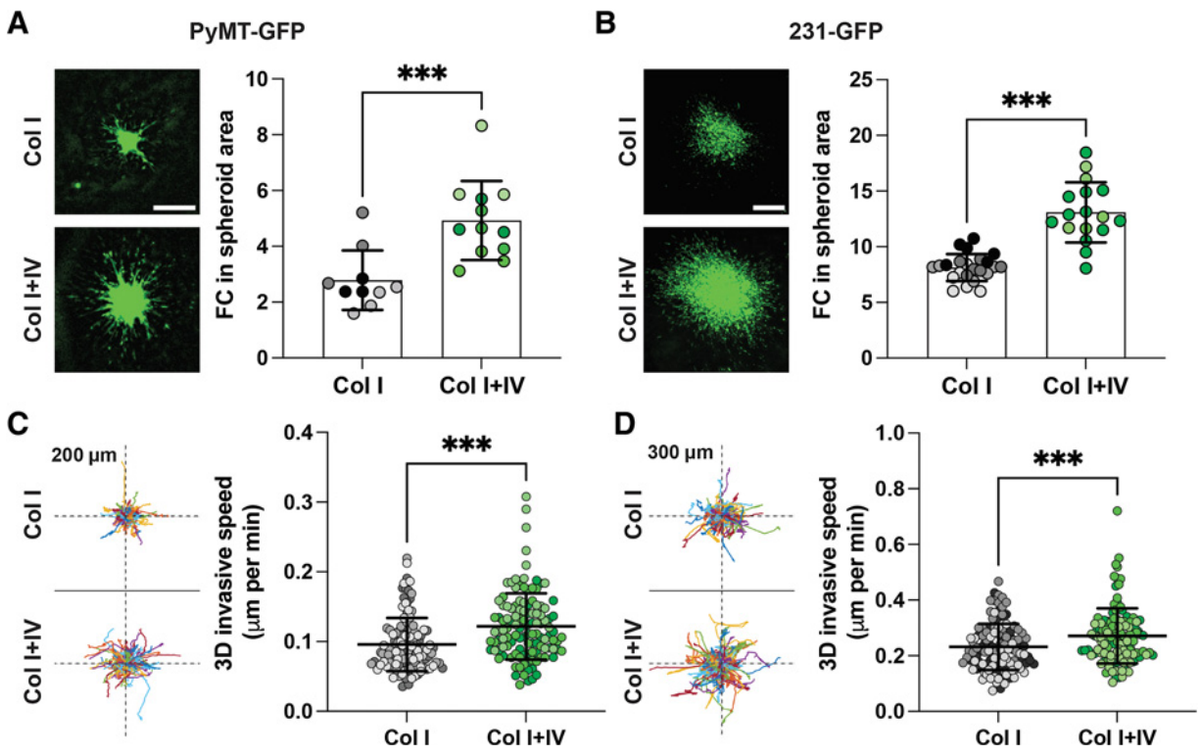

Figure 4.

Collagen IV drives spheroid growth and 3D invasion in mouse and human TNBC cells. **A,** Left, representative images of 3D TNBC spheroids of PyMT-GFP cells grown in collagen I (1 mg/mL) with or without collagen IV (20 μg/mL). Scale bar, 500 μm. Right, fold change (FC) in spheroid area was quantified. **B,** 3D TNBC spheroids of 231-GFP cells grown in the same conditions described. Scale bar, 500 μm. Fold change in spheroid area was quantified (right). Like-colored data points represent technical replicate spheroids grown on the same plate. **C,** Left, tracks of PyMT-GFP cells invading in collagen I (1 mg/mL) with or without collagen IV (20 μg/mL). Right, 3D invasive speed of cells was quantified. **D,** Tracks of 231-GFP cells invading in collagen I (1 mg/mL) with or without collagen IV (20 μg/mL, left). 3D invasive speed of cells was quantified. Data show mean ± SD [n = at least 9 spheroids from at least 3 independent experiments (**A** and **B**) or 120 cells from 3 independent experiments (**C** and **D**)]. Significance was determined by unpaired t test. ***, $P < 0.005$. Col I, collagen I; col I+IV, collagen I+IV; min, minute.

invasion in our models, we seeded PyMT-GFP or 231-GFP cells on full-length collagen IV–coated dishes for up to 2 hours. Analysis of phosphorylation status of collagen IV–associated signaling pathways revealed activation of Src, as measured by phosphorylation at Y416, and FAK, as measured by phosphorylation at Y397, in both PyMT-GFP (**Fig. 5A–C**) and 231-GFP cells (**Fig. 5D–F**). We found no activation of MAPK or PI3K pathways as measured by Erk1/2 phosphorylation at T202/204 and Akt phosphorylation at S473, respectively (Supplementary Fig. S5E–S5G).

The major receptors responsible for signaling downstream of native collagen IV are α1 and α2 integrins, which dimerize with β1 integrin to form functional adhesion receptors (45). As both α1β1 and α2β1 can effectively bind to both collagen I and collagen IV, we decided to use pooled siRNA-mediated knockdown to interrogate the relative contribution of ITGA1 and ITGA2 to collagen IV signaling in 231-GFP cells (Supplementary Fig. S6). Surprisingly, knockdown of ITGA1 alone had no effect on the signaling response to collagen IV, while knockdown of ITGA2 blocked activation of FAK, but not Src, in the presence of collagen IV (**Fig. 6A–C**). Only combined knockdown of ITGA1 and ITGA2 effectively suppressed collagen IV-driven Src activation, indicating compensatory signaling between these two receptors converging on Src.

Knockdown of integrin α1/α2 and inhibition of Src or FAK reduces collagen IV–driven 3D invasion

To determine if blunting the signaling response to collagen IV suppressed 3D invasion in collagen IV, we used ITGA1 and ITGA2 knockdown cells in single-cell 3D invasion studies. Surprisingly, ITGA1 knockdown increased 3D invasion independently of collagen IV (**Fig. 6D**). However, knockdown of ITGA2 alone or in combination with ITGA1 knockdown inhibited 3D invasion in response to collagen IV, consistent with our signaling studies (**Fig. 6D**). To investigate the importance of downstream Src/FAK signaling in collagen IV-driven 3D invasion, we leveraged existing small molecule inhibitors targeting Src (dasatinib) and FAK (defactinib). PyMT-GFP or 231-GFP spheroids were generated with or without collagen IV and treated with 10 nmol/L dasatinib or 1 μmol/L defactinib. These doses were chosen to detect anti-invasive effects while having minimal effect on cell proliferation or viability as described previously (46–48). In PyMT-GFP cells, inhibition of FAK, but not Src, reduced spheroid growth in collagen I, in the absence of collagen IV. However, inhibition of either Src or FAK blocked the collagen IV–driven increase in spheroid growth (**Fig. 7A** and **B**). Furthermore, while 231-GFP cells were insensitive to both Src and FAK inhibition in the absence of collagen IV, either drug ablated collagen IV-stimulated spheroid growth in

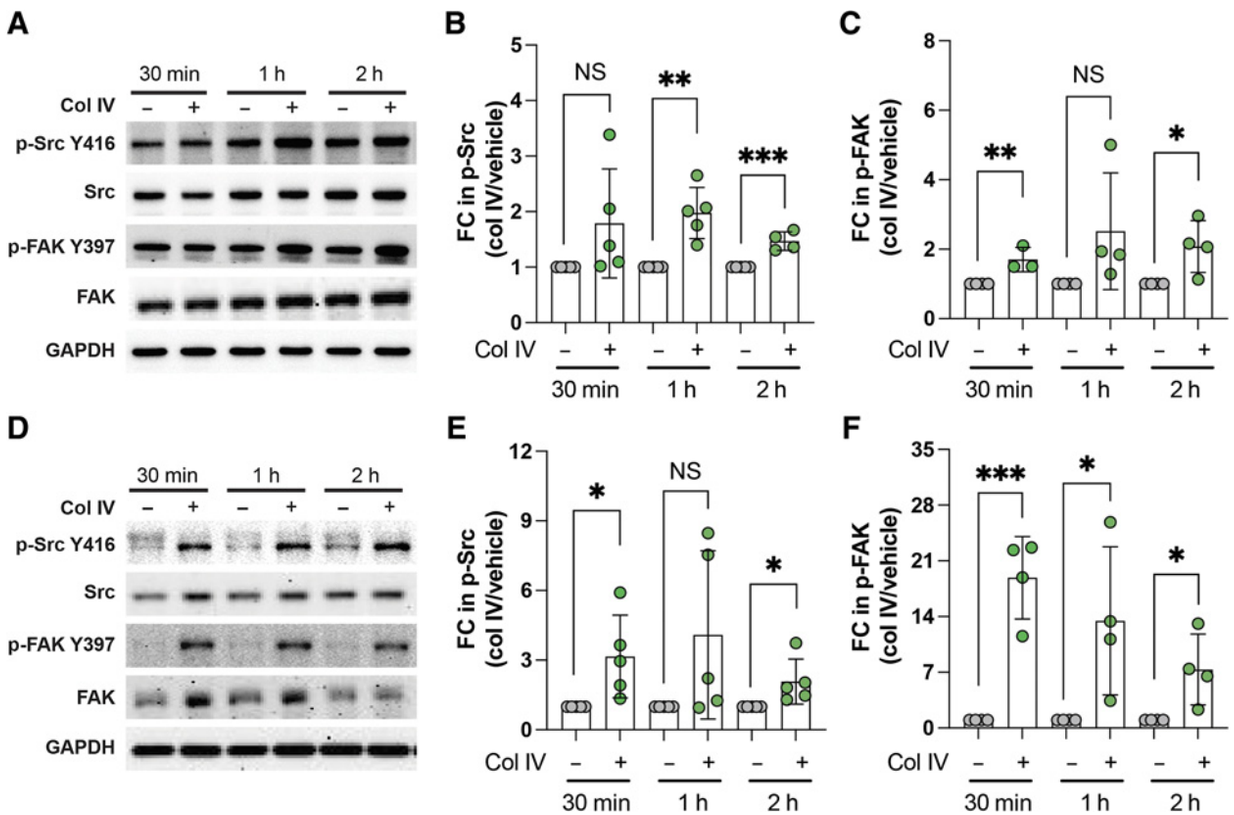

Figure 5.

Collagen IV activates Src and FAK signaling in mouse and human TNBC cells. Representative Western blot images of whole cell PyMT-GFP (**A**) or 231-GFP (**D**) lysates immunoblotted for the indicated proteins and phosphoproteins. Cells were plated on collagen IV–coated (20 μg/mL) or control dishes for the indicated times before lysis. Quantification of phospho-Src (Y416) signal in PyMT-GFP (**B**) or 231-GFP (**E**) cells relative to total Src protein and normalized to a loading control. Quantification of phospho-FAK (Y397) signal in PyMT-GFP (**C**) or 231-GFP (**F**) relative to total FAK and normalized to a loading control. Data show mean ± SD (n = at least 3 independent cell lysates.) Significance was determined by unpaired t test. *, $P < 0.05$; **, $P < 0.01$; ***, $P < 0.005$. Col IV, collagen IV; p-Src, phospho-Src; p-FAK, phospho-FAK; min, minutes; h, hours; NS, not significant.

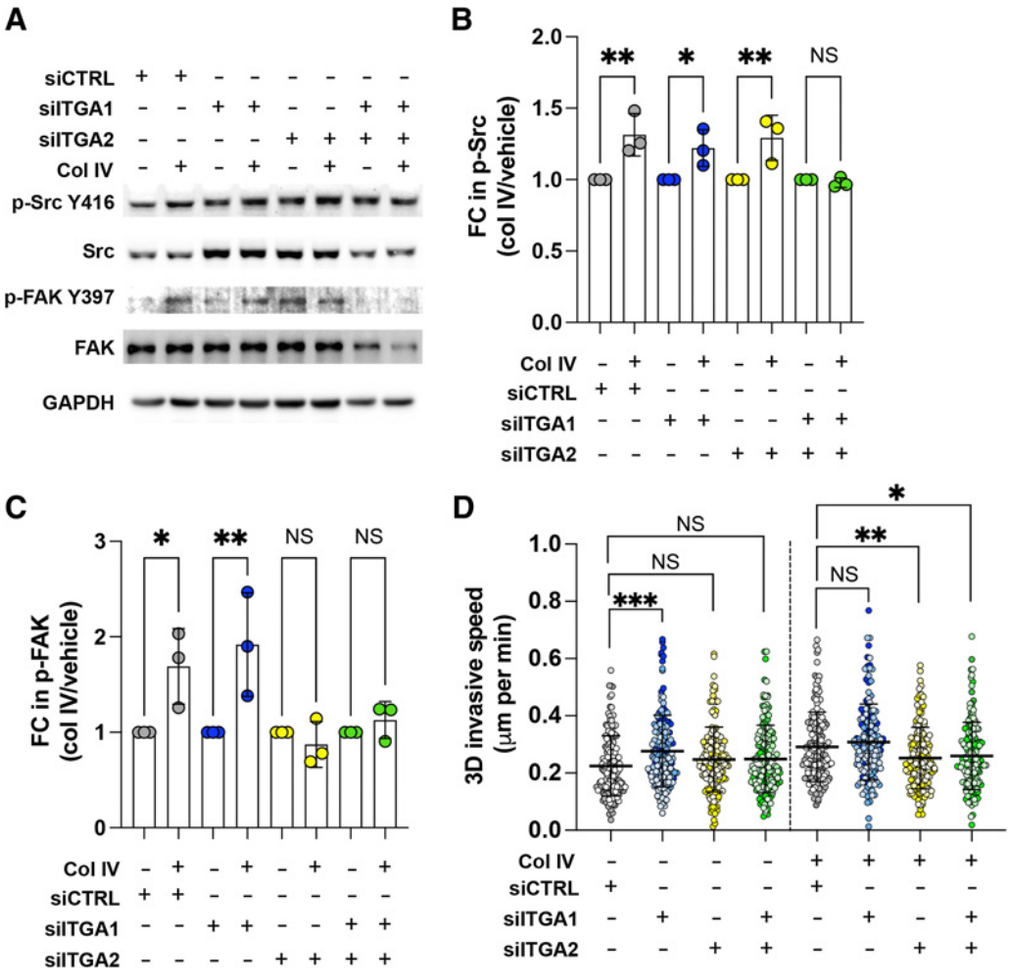

Figure 6.

Signaling and invasion downstream of collagen IV is mediated by α integrins in 231-GFP cells. **A,** Representative Western blots of signaling response to collagen IV with the indicated siRNA condition. **B,** Quantification of phospho-Src (Y416) signal relative to total Src protein and normalized to a loading control. **C,** Quantification of phospho-FAK(Y397) signal relative to total FAK protein and normalized to a loading control. **D,** 3D invasive speed of cells seeded in collagen I (1 mg/mL) with or without collagen IV (20 μg/mL) following the indicated siRNA transfections. Data show mean ± SD (n = at least 3 independent cell lysates (**A–E**) or at least 120 cells tracked from 3 independent experiments). Significance was determined by unpaired *t* test. *, $P < 0.05$; **, $P < 0.01$; ***, $P < 0.005$. Col IV, collagen IV; p-Src, phospho-Src; p-FAK, phospho-FAK; NS, not significant; min, minute; CTRL, control.

these cells as well (**Fig. 7C** and **D**). In single-cell 3D invasion studies, Src or FAK inhibition slowed PyMT-GFP invasion in collagen IV, but not collagen I alone (**Fig. 7E** and **F**). Similarly, inhibition of Src and FAK suppressed 231-GFP invasion in collagen IV, while only inhibition of Src slowed invasion in collagen I alone (**Fig. 7G** and **H**). These data collectively demonstrate that collagen IV–driven tumor cell invasion is dependent on α1/α2 integrins and activation of both Src and FAK.

Inhibition of collagen IV signaling suppresses chemotherapy-associated dECM-driven invasion

We last sought to confirm that collagen IV-driven signaling accounts for the increased motility driven by chemotherapy-treated dECM scaffolds identified in **Fig. 1**. PyMT-GFP or 231-GFP cells were seeded onto paclitaxel- and vehicle-treated dECM scaffolds and treated with 10 nmol/L dasatinib or 1 μmol/L defactinib, doses found to suppress collagen IV–driven invasion in our spheroid and single-cell invasion assays (**Fig. 7**). We found that neither drug suppressed movement of PyMT-GFP cells seeded on vehicle-treated dECM (**Fig. 8A** and **B**), while either drug alone effectively suppressed chemotherapy-associated increased motility of cells seeded on paclitaxel-treated dECM (**Fig. 8A** and **C**). 231-GFP cells displayed the same trend (**Fig. 8D–F**), confirming that Src and FAK signaling, which we find to be downstream of collagen IV, are essential for ECM-driven motility in postchemotherapy dECM scaffolds.

Discussion

Cytotoxic chemotherapy is an important tool that benefits many thousands of patients each year across cancer types. However, resistance to therapy and recurrence posttreatment occurs in over 25% of patients with TNBC. Therefore, it is essential that we gain a better understanding of the breadth of the systemic changes caused by these

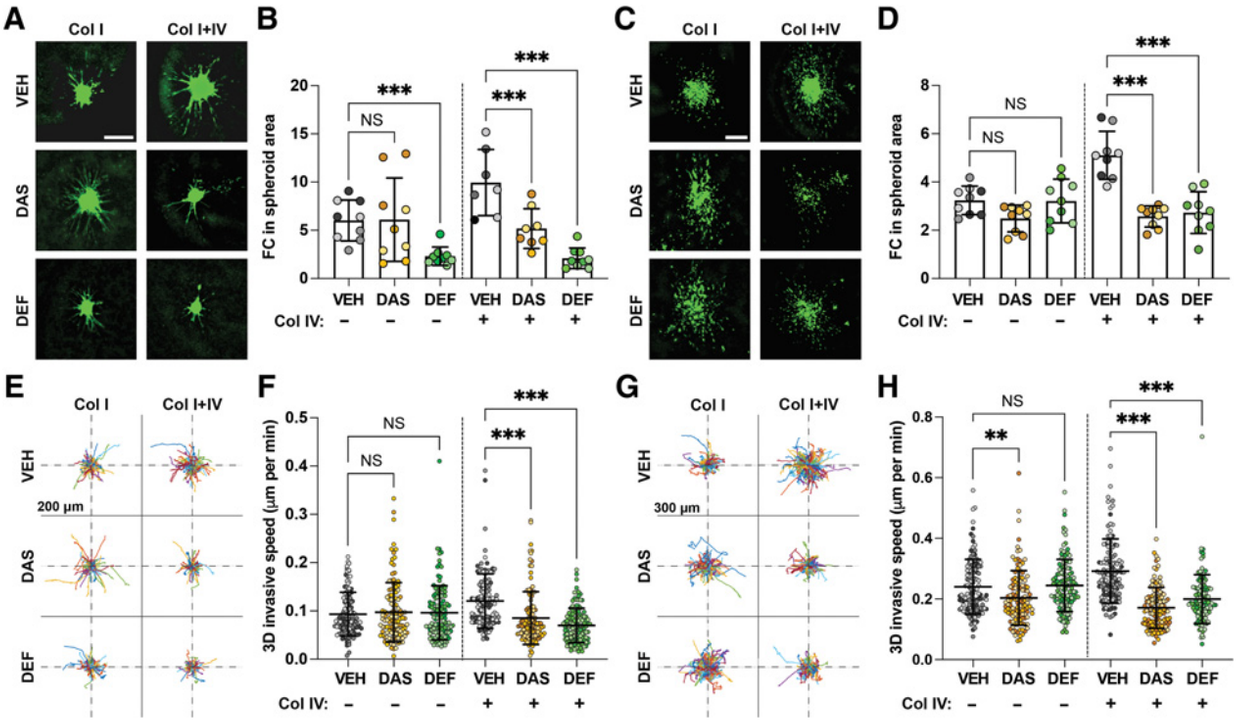

Figure 7.

Src or FAK inhibition ablates collagen IV–driven 3D invasion in TNBC cells. **A,** Representative images of PyMT-GFP spheroids grown with or without collagen IV and treated with DMSO (vehicle), 10 nmol/L dasatinib, or 1 µmol/L defactinib. Scale bar, 500 µm. **B,** Quantification of fold change in PyMT-GFP spheroid area after 4 days. **C,** Representative images of 231-GFP spheroids grown with or without collagen IV and treated with DMSO, 10 nmol/L dasatinib, or 1 µmol/L defactinib. Scale bar, 500 µm. **D,** Quantification of fold change in MDA-MB-231 spheroid area after 4 days. **E,** Tracks of PyMT-GFP cells invading with or without collagen IV and treated with DMSO, 10 nmol/L dasatinib, or 1 µmol/L defactinib. **F,** Quantification of 3D invasive speed of PyMT-GFP cells in **E**. **G,** Tracks of 231-GFP cells invading with or without collagen IV and treated with DMSO, 10 nmol/L dasatinib, or 1 µmol/L defactinib. **H,** Quantification of 3D invasive speed of 231-GFP cells in **G**. Like-colored data points represent technical replicate spheroids grown on the same plate or cells tracked in the same gel. Data show mean ± SD [$n = 7$–9 spheroids pooled from 3 independent experiments (**A–D**) or 120 cells tracked from three independent experiments (**E–H**)]. Significance was determined by one-way ANOVA. **, $P < 0.01$; ***, $P < 0.005$. Col I, collagen I; Col IV, collagen IV; Col I+IV, collagen I+IV; DAS, dasatinib; DEF, defactinib; min, minute; NS, not significant; VEH, vehicle.

therapies to maximize their clinical benefit and identify new clinical approaches to reduce the risk of chemotherapy-induced metastasis. While it is now understood that the ECM is an essential driver of tumor cell survival, invasion, and metastasis, the effect of chemotherapy on the ECM had not yet been investigated. Here, we report the first characterization of the chemotherapy-treated matrisome and identify collagen IV as a driver of cancer cell motility in the postchemotherapy tumor microenvironment. Importantly, we found that collagen IV expression was associated with increased likelihood of recurrence only in patients with breast cancer treated with cytotoxic chemotherapy, indicating that chemotherapy-induced collagen IV may be particularly conducive to TNBC recurrence. Using our dECM model, we further demonstrated that collagen IV–induced Src and FAK signaling were essential to cancer cell motility only in the context of chemotherapy-treated, collagen IV–rich dECM. Together, these data illustrate the first ECM-driven mechanism of chemotherapy-induced metastasis identified in TNBC.

Our study raises a number of questions about the microenvironmental response to NAC in TNBC. First, the mechanism by which chemotherapy stimulates collagen IV production *in vivo* is unclear. The apparent disparity between our proteomics and immunostaining data in doxorubicin-treated tumors may help us to understand potential mechanisms. It is well established that chemotherapy stimulates secretion of tumor-derived soluble signals leading to paracrine cross-talk between tumor and stromal cells (49). In this case, chemotherapy-induced production of ECM regulating enzymes may promote collagen IV trimerization without altering overall abundance of individual collagen IV chains. Proteomics studies have established that collagen IV is produced in similar amounts by both tumor and stromal cells *in vivo* (34), with fibroblasts, macrophages, and endothelial cells producing stromal collagen IV (24, 37, 50). Cui and colleagues found that cancer-associated fibroblasts produce collagen IV in response to taxane-based chemotherapy *in vitro*, but the mechanism is unknown (37). Studies investigating the direct and indirect effect of chemotherapy on collagen IV biosynthesis are underway in our lab. Further, our proteomics experiment identified a number of potentially prometastatic ECM proteins associated with chemotherapy that can serve as targets for future investigation. Paclitaxel treatment was associated with increased collagen VI abundance, which we have recently shown drives invasion in TNBC (31). Fibrillin was identified in paclitaxel-treated dECM, which, while understudied in breast cancer, has been shown to promote metastasis in ovarian cancer (51). In doxorubicin-treated dECM, we identified vitronectin and biglycan, two proteins known to promote invasiveness in cancer (52, 53). Further study is required to fully characterize the effect of these

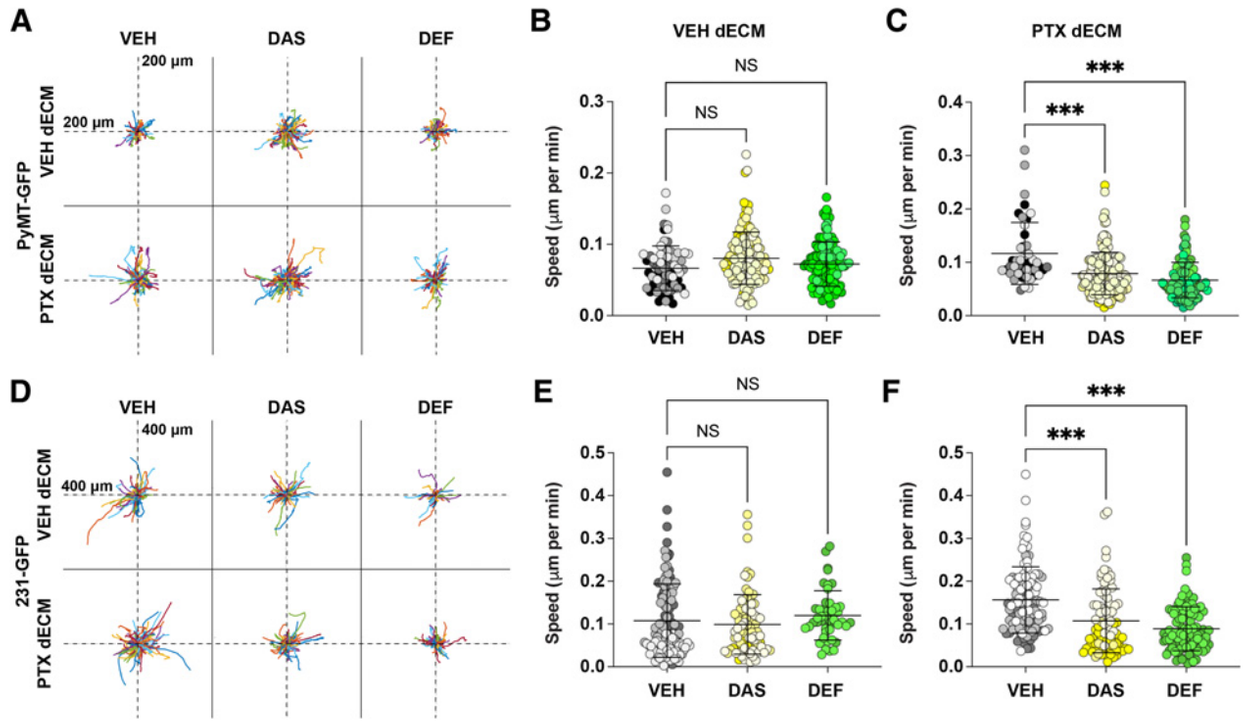

Figure 8.

Inhibition of Src or FAK suppresses chemotherapy-associated ECM-driven motility of TNBC cells. **A,** Rose plots depicting paths of individual PyMT-GFP cells seeded onto vehicle- or paclitaxel-treated dECM scaffolds and treated with DMSO (vehicle), 10 nmol/L dasatinib, or 1 μmol/L defactinib. **B,** Quantification of speed of PyMT-GFP cells seeded on vehicle-treated dECM. **C,** Quantification of speed of PyMT-GFP cells seeded on paclitaxel-treated dECM. **D,** Rose plots depicting paths of individual MDA-MB-231 cells seeded onto vehicle- or paclitaxel-treated dECM scaffolds and treated with DMSO, 10 nmol/L dasatinib, or 1 μmol/L defactinib. **E,** Quantification of speed of MDA-MB-231 cells seeded on vehicle-treated dECM. **F,** Quantification of speed of MDA-MB-231 cells seeded on paclitaxel-treated dECM. Each dot represents an individual tracked cell. Like-colored data points represent cell tracked from the same dECM scaffold. Data show mean ± SD (n = at least 45 cells tracked from at least 3 dECM scaffolds per treatment group). Significance was determined by one-way ANOVA. ***, $P < 0.005$. DAS, dasatinib; DEF, defactinib; min, minute; NS, not significant; VEH, vehicle.

complex chemotherapy-induced ECM changes on cancer cell phenotypes. While the present study focused on the compositional changes in ECM observed in the tumors, we also note an increase in tumor fibrosis induced by doxorubicin, which might further undermine clinical benefits by promoting local invasion or chemoresistance. Future studies are needed to evaluate the effect of chemotherapeutic drugs on the production of ECM or chemokines that may stimulate ECM production, by cells in the TME, as well as on the effect of chemotherapy on the biophysical properties of the ECM.

Overall, our work reveals a clinical paradigm where an increase in collagen IV induced by NAC may predispose some patients to suffer recurrence, which could be translated to patients in several ways. First, it is known that tumor-derived collagen IV can be detected in the serum of patients with breast cancer and that levels are increased during metastasis (35, 54). However, it is unknown if serum collagen IV levels correlate to tumor collagen IV abundance. Prospective study to interrogate the relationship between serum and tumor collagen IV during chemotherapy treatment may provide a noninvasive biomarker for detection of patients with chemotherapy-induced collagen IV. Further, the ECM is a promising target to facilitate drug delivery. Collagen-mimetic peptides have been developed that enable delivery of cargo to locations of high ECM turnover in the body, including to solid tumors (55). ECM-targeting antibodies have been developed that facilitate cargo delivery to tissues rich in specific ECM proteins (56). This technology could be used in patients with high collagen IV following chemotherapy to deliver metastasis-suppressing drugs.

Finally, we report that collagen IV–driven invasion in the post-chemotherapy TME may be counteracted using FDA-approved Src and FAK inhibitors, dasatinib and defactinib, respectively. Our data suggests that these drugs may suppress cancer cell dissemination in early stage TNBC, allowing for adjuvant chemotherapy to more effectively clear residual cancer cells. Dasatinib has been employed in combination with paclitaxel in breast cancer and has been shown to be well tolerated (57). However, clinical trials combining these drugs have been limited to patients with metastatic breast cancer (58). In one phase II study, 43% of patients showed either tumor regression or stable disease for greater than 6 months, but was discontinued due to slow patient accrual (58). While multiple phase I studies have demonstrated safety of defactinib in patients (59, 60), no completed studies have tested the efficacy of defactinib in combination with chemotherapy in breast cancer. The present study builds on existing preclinical literature demonstrating the efficacy of defactinib in overcoming chemoresistance (61), suppressing metastasis (62), and eliminating cancer stem cells (63) in a range of solid tumors. Taken together, our studies shed light on novel mechanisms of chemotherapy-induced metastasis in TNBC involving the ECM, that have the potential for clinical translation and development of new strategies to track, predict

and overcome drug resistance to prevent further metastasis and to reduce patient death.

Authors' Disclosures

J.P. Fatherree reports grants from NCI during the conduct of the study. S.P. Naber reports personal fees from Naveris, Inc. outside the submitted work. M.J. Oudin reports grants from NCI during the conduct of the study. No disclosures were reported by the other authors.

Authors' Contributions

J.P. Fatherree: Conceptualization, resources, data curation, formal analysis, supervision, funding acquisition, validation, investigation, visualization, methodology, writing–original draft, project administration, writing–review and editing. **J.R. Guarin:** Investigation, visualization, methodology, writing–review and editing. **R.A. McGinn:** Investigation, visualization, writing–review and editing. **S.P. Naber:** Investigation, visualization, methodology, project administration, writing–review and editing. **M.J. Oudin:** Conceptualization, supervision, funding acquisition, writing–original draft, project administration, writing–review and editing.

Acknowledgments

This work was supported by NIH (grant no. R00-CA207866 to M.J. Oudin), Tufts University (start-up funds from the School of Engineering to M.J. Oudin), and Tufts Graduate School of Biomedical Sciences (Collaborative Cancer Biology Award to J.P. Fatherree).

The costs of publication of this article were defrayed in part by the payment of page charges. This article must therefore be hereby marked *advertisement* in accordance with 18 U.S.C. Section 1734 solely to indicate this fact.

Received June 6, 2021; revised November 15, 2021; accepted March 4, 2022; published first March 8, 2022.

References

1. DeSantis CE, Ma J, Gaudet MM, Newman LA, Miller KD, Goding Sauer A, et al. Breast cancer statistics, 2019. CA Cancer J Clin 2019;69:438–51.
2. Bianchini G, Balko JM, Mayer IA, Sanders ME, Gianni L. Triple-negative breast cancer: challenges and opportunities of a heterogeneous disease. Nat Rev Clin Oncol 2016;13:674–90.
3. Schmid P, Rugo HS, Adams S, Schneeweiss A, Barrios CH, Iwata H, et al. Atezolizumab plus nab-paclitaxel as first-line treatment for unresectable, locally advanced or metastatic triple-negative breast cancer (IMpassion130): updated efficacy results from a randomised, double-blind, placebo-controlled, phase 3 trial. Lancet Oncol 2020;21:44–59.
4. Murphy BL, Day CN, Hoskin TL, Habermann EB, Boughey JC. Neoadjuvant chemotherapy use in breast cancer is greatest in excellent responders: triple-negative and HER2+ subtypes. Ann Surg Oncol 2018;25:2241–8.
5. Vriens BEPJ, Vriens IJH, Aarts MJB, van Gastel SM, van den Berkmortel FWPJ, Smilde TJ, et al. Improved survival for sequentially as opposed to concurrently delivered neoadjuvant chemotherapy in non-metastatic breast cancer. Breast Cancer Res Treat 2017;165:593–600.
6. Asselain B, Barlow W, Bartlett J, Bergh J, Bergsten-Nordström E, Bliss J, et al. Long-term outcomes for neoadjuvant versus adjuvant chemotherapy in early breast cancer: meta-analysis of individual patient data from ten randomised trials. Lancet Oncol 2018;19:27–39.
7. Ibragimova MK, Tsyganov MM, Litviakov NV. Natural and chemotherapy-induced clonal evolution of tumors. Biochemistry 2017;82:413–25.
8. Balko JM, Giltnane JM, Wang K, Schwarz LJ, Young CD, Cook RS, et al. Molecular profiling of the residual disease of triple-negative breast cancers after neoadjuvant chemotherapy identifies actionable therapeutic targets. Cancer Discov 2014;4:232–45.
9. Stover DG, Coloff JL, Barry WT, Brugge JS, Winer EP, Selfors LM. The role of proliferation in determining response to neoadjuvant chemotherapy in breast cancer: a gene expression-based meta-analysis. Clin Cancer Res 2016;22:6039–50.
10. Shaked Y, Henke E, Roodhart JML, Mancuso P, Langenberg MHG, Colleoni M, et al. Rapid chemotherapy-induced acute endothelial progenitor cell mobilization: implications for antiangiogenic drugs as chemosensitizing agents. Cancer Cell 2008;14:263–73.
11. Shaked Y. Therapy-induced acute recruitment of circulating endothelial progenitor cells to tumors. Science 2006;313:1785–7.
12. Volk-Draper L, Hall K, Griggs C, Rajput S, Kohio P, DeNardo D, et al. Paclitaxel therapy promotes breast cancer metastasis in a TLR4-dependent manner. Cancer Res 2014;74:5421–34.
13. DeNardo DG, Brennan DJ, Rexhepaj E, Ruffell B, Shiao SL, Madden SF, et al. Leukocyte complexity predicts breast cancer survival and functionally regulates response to chemotherapy. Cancer Discov 2011;1:54–67.
14. Nakasone ES, Askautrud HA, Kees T, Park JH, Plaks V, Ewald AJ, et al. Imaging tumor-stroma interactions during chemotherapy reveals contributions of the microenvironment to resistance. Cancer Cell 2012;21:488–503.
15. Peiris-Pagès M, Sotgia F, Lisanti M. Chemotherapy induces the cancer-associated fibroblast phenotype, activating paracrine Hedgehog-GLI signalling in breast cancer cells. Oncotarget 2015;6:10728–45.
16. Cox TR. The matrix in cancer. Nat Rev Cancer 2021;21:217–38.
17. Insua-Rodríguez J, Oskarsson T. The extracellular matrix in breast cancer. Adv Drug Deliv Rev 2016;97:41–55.
18. Lu P, Weaver VM, Werb Z. The extracellular matrix: a dynamic niche in cancer progression. J Cell Biol 2012;196:395–406.
19. Provenzano PP, Inman DR, Eliceiri KW, Knittel JG, Yan L, Rueden CT, et al. Collagen density promotes mammary tumor initiation and progression. BMC Med 2008;6:1–15.
20. Brabrand A, Kariuki II, Engstrøm MJ, Haugen OA, Dyrnes LA, Åsvold BO, et al. Alterations in collagen fibre patterns in breast cancer. A premise for tumour invasiveness? APMIS 2015;123:1–8.
21. Naba A, Clauser KR, Ding H, Whittaker CA, Carr SA, Hynes RO. The extracellular matrix: tools and insights for the "omics" era. Matrix Biol 2016;49:10–24.
22. Naba A, Clauser KR, Hoersch S, Liu H, Carr SA, Hynes RO. The matrisome: in silico definition and in vivo characterization by proteomics of normal and tumor extracellular matrices. Mol Cell Proteomics 2012;11:1–18.
23. Alkasalias T, Moyano-Galceran L, Arsenian-Henriksson M, Lehti K. Fibroblasts in the tumor microenvironment: shield or spear? Int J Mol Sci 2018;19:1–21.
24. Afik R, Zigmond E, Vugman M, Klepfish M, Shimshoni E, Pasmanik-Chor M, et al. Tumor macrophages are pivotal constructors of tumor collagenous matrix. J Exp Med 2016;213:2315–31.
25. Sun Z, Wang C-Y, Lawson DA, Kwek S, Velozo HG, Owyong M, et al. Single-cell RNA sequencing reveals gene expression signatures of breast cancer-associated endothelial cells. Oncotarget 2018;9:10945–61.
26. Tian C, Clauser KR, Öhlund D, Rickelt S, Huang Y, Gupta M, et al. Proteomic analyses of ECM during pancreatic ductal adenocarcinoma progression reveal different contributions by tumor and stromal cells. Proc Natl Acad Sci U S A 2019;116:19609–18.
27. Chou JL, Shen ZX, Waxman S, Stolfi RL, Martin DS. Effects of extracellular matrix on the growth and casein gene expression of primary mouse mammary tumor cells in vitro. Cancer Res 1989;49:5371–6.
28. Malik R, Luong T, Cao X, Han B, Shah N, Franco-Barraza J, et al. Rigidity controls human desmoplastic matrix anisotropy to enable pancreatic cancer cell spread via extracellular signal-regulated kinase 2. Matrix Biol 2019;81:50–69.
29. Balion Z, Sipailaite E, Stasyte G, Vailionyte A, Mazetyte-Godiene A, Seskeviciute I, et al. Investigation of cancer cell migration and proliferation on synthetic extracellular matrix peptide hydrogels. Front Bioeng Biotechnol 2020;8:1–13.
30. Hoshiba T. Decellularized extracellular matrix for cancer research. Materials 2019;12:1–16.
31. Wishart AL, Conner SJ, Guarin JR, Fatherree JP, Peng Y, McGinn RA, et al. Decellularized extracellular matrix scaffolds identify full-length collagen VI as a driver of breast cancer cell invasion in obesity and metastasis. Sci Adv 2020;6:eabc3175.
32. Baskaran JP, Weldy A, Guarin J, Munoz G, Shpilker PH, Kotlik M, et al. Cell shape, and not 2D migration, predicts extracellular matrix-driven 3D cell invasion in breast cancer. APL Bioeng 2020;4:026105.

33. Lin EY, Jones JG, Li P, Zhu L, Whitney KD, Muller WJ, et al. Progression to malignancy in the polyoma middle T oncoprotein mouse breast cancer model provides a reliable model for human diseases. Am J Pathol 2003; 163:2113–26.
34. Naba A, Clauser KR, Lamar JM, Carr SA, Hynes RO. Extracellular matrix signatures of human mammary carcinoma identify novel metastasis promoters. Elife 2014;2014:1–23.
35. Lindgren M, Jansson M, Tavelin B, Dirix L, Vermeulen P, Nyström H. Type IV collagen as a potential biomarker of metastatic breast cancer. Clin Exp Metastasis 2021;38:175–85.
36. Knutson JR, Iida J, Fields GB, McCarthy JB. CD44/chondroitin sulfate proteoglycan and α2β1 integrin mediate human melanoma cell migration on type IV collagen and invasion of basement membranes. Mol Biol Cell 1996;7:383–96.
37. Cui Q, Wang B, Li K, Sun H, Hai T, Zhang Y, et al. Upregulating MMP-1 in carcinoma-associated fibroblasts reduces the efficacy of taxotere on breast cancer synergized by collagen IV. Oncol Lett 2018;16:3537–44.
38. Nagy Á, Lánczky A, Menyhárt O, Gyorffy B. Validation of miRNA prognostic power in hepatocellular carcinoma using expression data of independent datasets. Sci Rep 2018;8:1–9.
39. Wu P-H, Gambhir SS, Hale CM, Chen W-C, Wirtz D, Smith BR. Particle tracking microrheology of cancer cells in living subjects. Mater Today 2020;39:98–109.
40. Crowe DL, Ohannessian A. Recruitment of focal adhesion kinase and paxillin to β1 integrin promotes cancer cell migration via mitogen activated protein kinase activation. BMC Cancer 2004;4:1–8.
41. Favreau AJ, Vary CPH, Brooks PC, Sathyanarayana P. Cryptic collagen IV promotes cell migration and adhesion in myeloid leukemia. Cancer Med 2014;3: 265–72.
42. Robledo T, Arriaga-Pizano L, Lopez-Pérez M, Salazar EP. Type IV collagen induces STAT5 activation in MCF7 human breast cancer cells. Matrix Biol 2005; 24:469–77.
43. Castro-Sanchez L, Soto-Guzman A, Guaderrama-Diaz M, Cortes-Reynosa P, Salazar EP. Role of DDR1 in the gelatinases secretion induced by native type IV collagen in MDA-MB-231 breast cancer cells. Clin Exp Metastasis 2011;28: 463–77.
44. Burnier JV, Wang N, Michel RP, Hassanain M, Li S, Lu Y, et al. Type IV collagen-initiated signals provide survival and growth cues required for liver metastasis. Oncogene 2011;30:3766–83.
45. Khoshnoodi J, Pedchenko V, Hudson BG. Mammalian collagen IV. Microsc Res Tech 2008;71:357–70.
46. Tranchant R, Quetel L, Montagne F, De Wolf J, Meiller C, De Koning L, et al. Assessment of signaling pathway inhibitors and identification of predictive biomarkers in malignant pleural mesothelioma. Lung Cancer 2018;126:15–24.
47. Kanteti R, Mirzapoiazova T, Riehm JJ, Dhanasingh I, Mambetsariev B, Wang J, et al. Focal adhesion kinase a potential therapeutic target for pancreatic cancer and malignant pleural mesothelioma. Cancer Biol Ther 2018;19:316–27.
48. Schönholzer MT, Migliavacca J, Alvarez E, Santhana Kumar K, Neve A, Gries A, et al. Real-time sensing of MAPK signaling in medulloblastoma cells reveals cellular evasion mechanism counteracting dasatinib blockade of ERK activation during invasion. Neoplasia 2020;22:470–83.
49. Maia A, Gu Z, Koch A, Berdiel-Acer M, Will R, Schlesner M, et al. IFNβ1 secreted by breast cancer cells undergoing chemotherapy reprograms stromal fibroblasts to support tumour growth after treatment. Mol Oncol 2021;15:1308–29.
50. Ojima K, Oe M, Nakajima I, Muroya S, Nishimura T. Dynamics of protein secretion during adipocyte differentiation. FEBS Open Bio 2016;6:816–26.
51. Wang Z, Liu Y, Lu L, Yang L, Yin S, Wang Y, et al. Fibrillin-1, induced by Aurora-A but inhibited by BRCA2, promotes ovarian cancer metastasis. Oncotarget 2015;6:6670–83.
52. Schneider G, Bryndza E, Poniewierska-Baran A, Serwin K, Suszynska M, Sellers ZP, et al. Evidence that vitronectin is a potent migration-enhancing factor for cancer cells chaperoned by fibrinogen: a novel view of the metastasis of cancer cells to low-fibrinogen lymphatics and body cavities. Oncotarget 2016;7:69829–43.
53. Sun H, Wang X, Zhang Y, Che X, Liu Z, Zhang L, et al. Biglycan enhances the ability of migration and invasion in endometrial cancer. Arch Gynecol Obstet 2016;293:429–38.
54. Mazouni C, Arun B, André F, Ayers M, Krishnamurthy S, Wang B, et al. Collagen IV levels are elevated in the serum of patients with primary breast cancer compared to healthy volunteers. Br J Cancer 2008;99:68–71.
55. Yasui H, Yamazaki CM, Nose H, Awada C, Takao T, Koide T. Potential of collagen-like triple helical peptides as drug carriers: their in vivo distribution, metabolism, and excretion profiles in rodents. Biopolymers 2013;100:705–13.
56. Jailkhani N, Ingram JR, Rashidian M, Rickelt S, Tian C, Mak H, et al. Noninvasive imaging of tumor progression, metastasis, and fibrosis using a nanobody targeting the extracellular matrix. Proc Natl Acad Sci U S A 2019;116:14181–90.
57. Ocana A, Gil-Martin M, Martín M, Rojo F, Antolín S, Guerrero Á, et al. A phase I study of the SRC kinase inhibitor dasatinib with trastuzumab and paclitaxel as first line therapy for patients with HER2-overexpressing advanced breast cancer. GEICAM/2010-04 study. Oncotarget 2017;8:73144–53.
58. Morris PG, Rota S, Cadoo K, Zamora S, Patil S, D'Andrea G, et al. Phase II study of paclitaxel and dasatinib in metastatic breast cancer. Clin Breast Cancer 2018; 18:387–94.
59. Jones SF, Siu LL, Bendell JC, Cleary JM, Razak ARA, Infante JR, et al. A phase i study of VS-6063, a second-generation focal adhesion kinase inhibitor, in patients with advanced solid tumors. Invest New Drugs 2015;33:1100–7.
60. Shimizu T, Fukuoka K, Takeda M, Iwasa T, Yoshida T, Horobin J, et al. A first-in-asian phase 1 study to evaluate safety, pharmacokinetics and clinical activity of vs-6063, a focal adhesion kinase (FAK) inhibitor in Japanese patients with advanced solid tumors. Cancer Chemother Pharmacol 2016;77:997–1003.
61. Lin H, Lee BY, Castillo L, Spielman C, Grogan J, Yeung NK, et al. Effect of FAK inhibitor VS-6063 (defactinib) on docetaxel efficacy in prostate cancer. Prostate 2018;78:308–17.
62. Zhang L, Zhao D, Wang Y, Zhang W, Zhang J, Fan J, et al. Focal adhesion kinase (FAK) inhibitor-defactinib suppresses the malignant progression of human esophageal squamous cell carcinoma (ESCC) cells via effective blockade of PI3K/AKT axis and downstream molecular network. Mol Carcinog 2021;60: 113–24.
63. Kolev VN, Tam WF, Wright QG, McDermott SP, Vidal CM, Shapiro IM, et al. Inhibition of FAK kinase activity preferentially targets cancer stem cells. Oncotarget 2017;8:51733–47.